ADSORPTIVE APPROACH ON NEPHOLOMETRIC STUDY OF PAINT EFFLUENT USING *TYMPANOTONOS FUSCATUS* EXTRACT

Ifechukwu G. Ezemagu[1], Matthew C. Menkiti[1,2*], Victor I. Ugonabo[1] and Mathew C. Aneke[3]

[1]Department of Chemical Engineering, Nnamdi Azikiwe University, Awka, Nigeria
[2]Water Resources Center, Texas Tech University, Lubbock, Texas, USA
[3]Department of Chemical Engineering, University of Hull, UK

ABSTRACT. Adsorptive study of paint effluent coagulation using *T. fuscatus* coagulant (TFC) is investigated. Effects of pH, dose, time, and temperature were investigated. Functional group, crystalline, morphology and thermal characteristics of samples were determined. Equilibrium data were analysed by Langmuir, Freundlich, Temkin, Frumkin, and Dubinin-Radushkevich (D-R) isotherms. Kinetic data were fitted to reversible first order, pseudo-first-order, pseudo-second-order, Elovich, intra-particle diffusion and Boyd kinetic models. Process Gibbs free energy (ΔG°), enthalpy (ΔH°) and the entropy (ΔS°) were evaluated. The process was best described by Langmuir isotherm ($R^2 > 0.99$; $X^2 < 0.6$; SSE < 0.7). Pseudo second order best fitted the kinetic data. The process was spontaneous, feasible and endothermic. 97% optimal removal was achieved at pH 5. *Tympanotonos fuscatus* extract has potential for application as an effective coagulant while showing significant component of adsorptive phenomenon

KEY WORDS: Paint effluent, Coagulation/flocculation, Adsorption, *Tympanotonos fuscatus*

INTRODUCTION

Industrialization has accelerated pollution in the aquifers, such that much of the water requires a form of treatment before use. Paint effluent (PE) contributes to this pollution. PE is turbid and contains highly toxic compounds that harm humans, fishes and contaminates the food chain if drained into soil [1, 2]. Thus, the treatment and safe disposal of PE become vital for environmental conservation.

The treatment methods are selective and include chemical precipitation, adsorption, ion exchange and coagulation/flocculation, which had been implemented using varieties of coagulants and effluents [3-7]. The advantage is that coagulation is robust, relatively low energy demand, needs low operator skill and active in natural organic matter (NOM), inorganics and turbidity enriched effluent.

Factors that affect coagulation include raw effluent characteristics, temperature, pH, dosage, etc [8]. Traditionally, coagulation-flocculation has been achieved using inorganic alum and iron chloride. Problems with their usage include poor performance in low-temperature water and high sludge volume generation and link to Alzheimer's disease in human [9]. These problems motivated the use of extracts from snail shell, nirmali seeds (*Strychnos potatorum*), *Moringa oleifera*, tannin, cactus [10] and *T. fuscatus* shell.

T. fuscatus shell (TFS) is of natural non-toxic chitin, which is a major component of the shells of crustacean. It is enriched with carbohydrate biopolymer [11, 12]. TFS abound as wastes in Nigeria, making it attractive as biomaterials. *T. fuscatus* coagulant (TFC), obtained by deacetylation of chitin [11, 12], has been applied in varying effluents and could be extended to PE.

Currently, there is little study focus on adsorptive component of bio-coagulation, hence this report contributes towards bridging this gap. Coagulation data were analysed in the light of

_____

adsorption isotherm, kinetics and thermodynamics. Effects of process variables were evaluated. Instrumental and physiochemical characterization of sample were conducted.

EXPERIMENTAL

Material collection and preparation

PE and TFS were obtained from Onitsha, Anambra State, Nigeria. PE was prepared and stored [13-15]. TFS was processed to TFC [11, 16]**.** The processing involved majorly: deproteinization, demineralization and deacetylation to produce TFC.

Material characterization

Paint effluent. Standard APHA methods [15] were applied for physiochemical characterization of PE.

T. fuscatus shell. Yield/weight loss, bulk density, ash content, oil content, moisture content and protein content were determined as reported elsewhere [17].

Instrumental characterization of bio-coagulant. Instrumental characterization was conducted using Thermo Nicolet Nexus 470/670/870 FTIR Spectrophotometer, Philips X PERT X-RAY diffractometer, Zeiss Evo®MA 15 EDX/WDS microscope and (TGA – Q50 and DSC – Q200) theremogravimetric units.

Coagulation and flocculation experiment

Effect of coagulant dosage on efficiency. Initial pH and turbidity of PE were determined. (i) 1000 mL of the PE contained in 10 different 1000 mL GG-17 beakers (10 cm diameter) were dosed with 0.50–5 g/L of TFC. (ii) Using magnetic stirrer, the mixture of the effluent and coagulant contained in the 1000 mL beakers were subjected to rapid mixing at 250 rpm (G = 550 s^{-1}) for 2 min, followed by slow mixing at 30 rpm (G = 22 s^{-1}) for 20 min. (iii) At the end of slow mixing, the treated PE was allowed to settle for 30 min. (iv) At 30 min settling time, 20 mL of the supernatant was respectively pipetted from 2 cm depth into 50 mL turbidity cuvette and residual turbidity measured for each dosage for the determination of optimum dosage.

Effect of pH variation on efficiency. The optimum dosage obtained from results was used for the evaluation of pH effect. The following steps were involved: (i) Equal optimum dosages of TFC were dosed into 9 different beakers each containing 1000 mL of PE sample. The samples pH was adjusted to 2, 3, 4, 5, 6, 7, 8, 9 and 10 using 0.1 M H_2SO_4 and 0.1 M NaOH just before dosing of the coagulant sample. (ii) Steps (ii-iv) in the previous subsection were repeated with respect to pH variation, leading to determination of optimum pH.

Temporal variation of Q_t with dosage. (i) Steps (i)-(ii) were repeated. (ii) During the settling period following the ceasing of slow mixing, 20 mL of the supernatant was respectively pipetted from 2 cm depth into 50 mL turbidity cuvette at 3, 5, 10, 15, 20, 25 and 30 min. The residual turbidity of each supernatant collected was measured and converted to mg/L on multiplying turbidity by a conversion factor of 2.35 [13].

Analytical method

The adsorptive capacity, q_t (mg/g), and the percentage removal, % Rem, were calculated using Eqs. 1 and 2, respectively.

$$q_t = \frac{Co-Ct)}{M} x\, V \tag{1}$$

$$\%Rem = \frac{Co-Ct}{Co} x\, 100 \tag{2}$$

where C_o, C_t V and M are initial constant effluent concentration (mg/L), effluent concentration at any time, t; volume of effluent (l) and mass of coagulant (g), respectively.

RESULTS AND DISCUSSION

Characterization results

Physiochemical and biological characteristics. Characteristics of TFS and PE along with the regulatory standard are presented in Tables 1 and 2, respectively. Total suspended solid, total dissolved solid and total solid of PE were relatively significant to support coagulation study. Meanwhile, the protein content of TFS was substantial to suggest TFS as precursor.

Table 1. Proximate analysis of TFS.

Parameter	Value
Yield (%)	80
Weight loss (%)	20
Bulk density (g/mL)	0.12
Ash content (%)	4.98
Oil content (%)	10
Moisture content (%)	4.5
Protein (%)	17.7

Table 2. PE characteristics and NESRA[*] standard.

Parameter	Value	NESRA
TSS	2679 mg/L	100 mg/L
pH	8	6-8
TDS	1365 mg/L	1200 mg/L
TS	4044 mg/L	1300 mg/L

[*]National Environment Standards Regulations (NESRA), Nigeria.

FTIR spectra analyses. FTIR spectrum of TFC shown in Figure 1 exhibits 19 discernable peaks at 600–4000 cm^{-1} with a threshold of 1.17. In Figure 1, peaks at 3850 to 3593 cm^{-1} could be attributed to hydroxyl (O–H) groups. Peak at 3296 cm^{-1} is linked to secondary amide (N–H) groups. Peaks at 2916 and 2850 cm^{-1} are for aliphatic hydrocarbon. Aliphatic rings (C=C stretching, NH$_2$ scissoring, azo compound and N–H bending) were peaked at 1634 to 1443 cm^{-1}. Peaks at 1082, 1068 and 1032 cm^{-1} are for C–O stretching. Amine and alkyne peaks at 909, 855, 781, 712 and 699 cm^{-1} are for N–H stretching, NH$_2$ wagging and twisting, N–H wagging and =C–H bending, respectively [18].

XRD pattern. The XRD pattern of TFC shown in Figure 2 depicts eleven clear peaks. Some of the crystal peaks were shifted towards left-right axes, resulting from expansion or contraction of

the sample. The peaks indicated that the atomic structure of TFC was of primitive lattice structure.
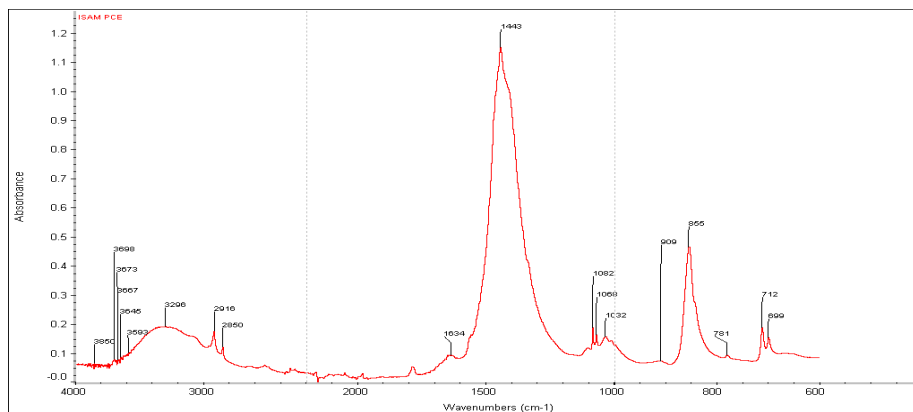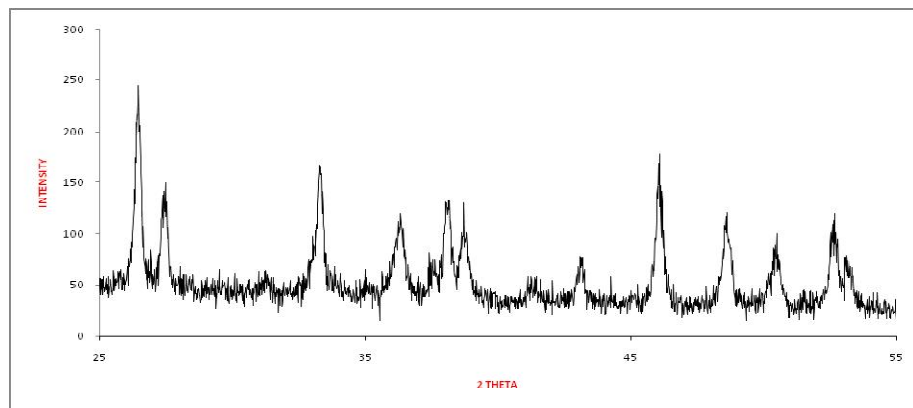

Figure 1. FTIR spectrum of TFC.

Figure 2. XRD pattern of TFC.

Thermo-gravimetric and differential scanning calorimetric analyses. The TGA and DSC curves for TFC are presented in Figure 3. The weight loss of the material could result from chemical reaction (decomposition, combustion) and physitransition (evaporation, desorption, drying) [19, 20]. Figure 3a indicates that the final residual mass was 3.26 mg (94.1% original weight). In Figure 3a, the initial weight loss resulted from the internal moisture and gaseous losses [21]. The second phase weight loss resulted from the decomposition of the labile component in the samples. Figure 3b indicates phase transition involving two eutectic peaks at 37.5–297 °C for enthalpy of 11.4 kJ/mol. The endothermic densification took place at 112.5–187.5 °C (Figure 3b). Figure 3b indicates glass transition temperature within 31.25–37.5 °C for the coiling of carbon chain necessary for spontaneous densification [21, 22]. Conclusively, Figure 3 suggested thermal operational stability at activation energy of 15.0 kJ/mol. Figure 3b indicated exothermicity.
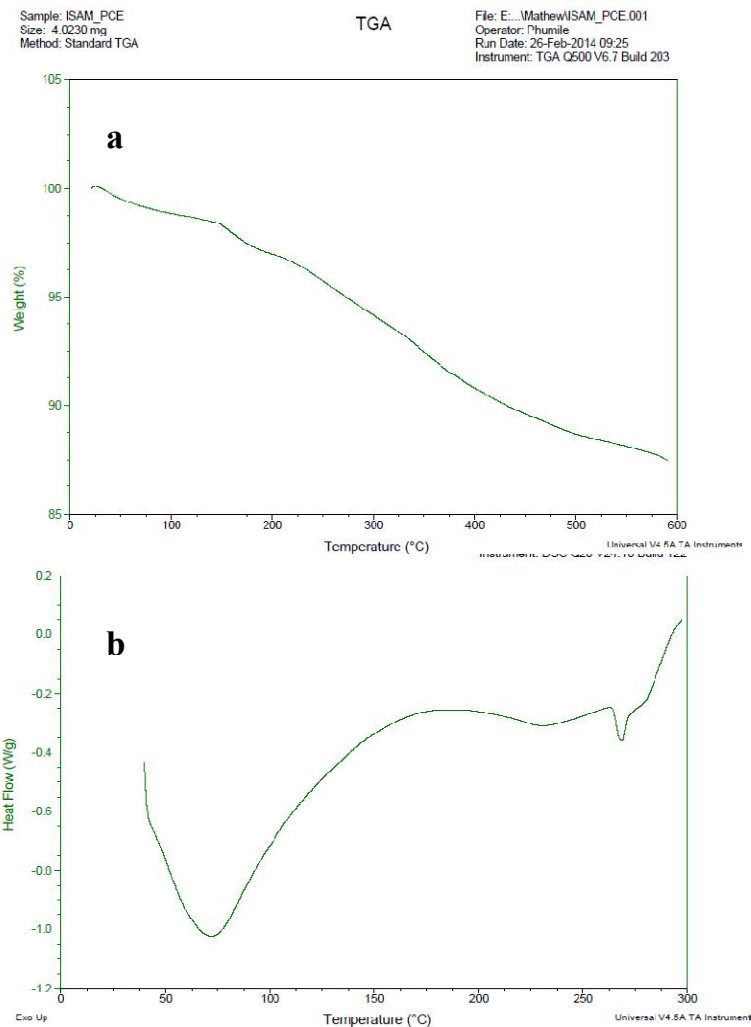
Figure 3. (a) TGA and (b) DSC of TFC.

SEM analyses. The surface morphology of TFC is shown in Figure 4. The images in Figure 4 appear to be white field with porous but irregular network structure. While Figure 4a indicates the penetrating pores towards the internals of the sample mass, Figure 4b shows the discrete multiple pores of the sample. The prevalence of these pores activated the binding affinity among the coagulant's pores surfaces and effluent's particles.
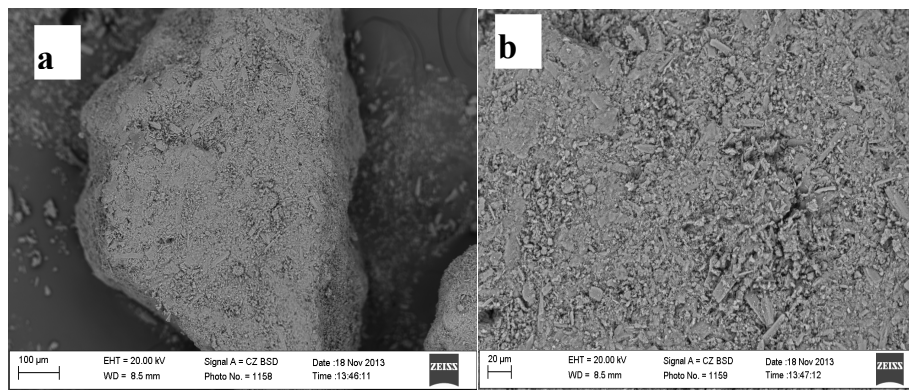
Figure 4. SEM micrograph of TFC.

Factors sensitivity analysis

Effect of TFC dosage on particle removal efficiency. Figure 5 indicates (at natural pH) that the efficiency increased from 4% at 0.5 g/L, peaking at 46.6% for 2 g/L and thereafter decreased to 6% at 5 g/L. The increase resulted from increased supply of coagulant's charged species (mainly +ve charges) that incrementally destabilized the effluent charged species (mainly -ve charges), thus ensuring progressive particle removal as dosage increased from 0.5 to 2 g/L. Furthermore, the decrease after 2 g/L resulted from sustained re-stabilisation following excessive supply of +ve charged species due to overdosing after 2 g/L, up till 5 g/L. At 2 g/L, both charged species equilibrated for optimum performance [8, 23]. Hence, 2 g/L applied for the effect of pH.

Effect of pH on particle removal at 2 g/L TFC. The effect of pH on efficiency for optimum 2 g/L TFC is depicted in Figure 6. Figure 6 exhibited alternate decrease and increase in efficiency as the pH decreased from 9-2. The pH ranges 3-2 and 8-5 recorded increment in efficiency due to progressive protonation. Conversely, the decrease in efficiency for pH ranges 9-8 and 5-3 could be explained by net +ve and –ve species induced charge reversal, respectively. Charge reversal results in re-stabilization and coagulation retardation. Optimal 97% at pH 5 denoted equilibrium in the provision of opposing ions for point of zero charge [23].
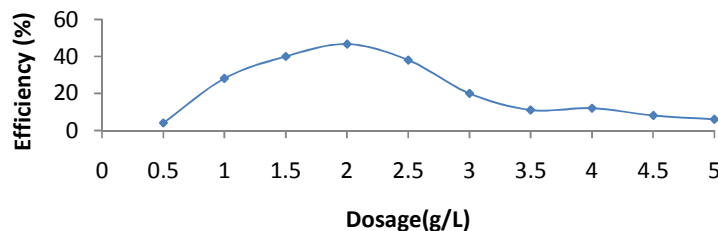

Figure 5. Removal efficiency vs dosage for TFC in PE.

Temporal variation of adsorption capacity for TFC in PE. The q_t of TFC is shown in Figure 7. It shows that ~ 90% of adsorption occurred between 0–20 min; thereafter q_t became constant [21]. Meanwhile, Figure 7, demonstrated that q_t increased with decreasing dosage and increasing

time. At 0.5 and 5 g/L, the highest and the lowest values of q_t were respectively, recorded. q_t at 0.5 g/L increased from 372 to 471 mg/g for 0 and (20-30) min, respectively. At 5 g/L, q_t increased from 230 to 253 mg/g for 0 and (20-30) min, respectively.
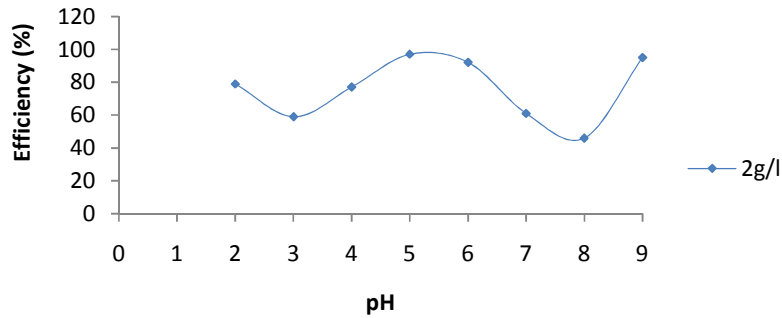

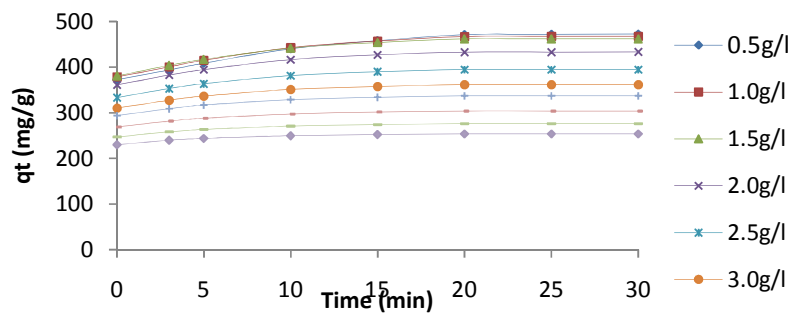Figure 6. Effect of pH on particle removal efficiency at 2 g/L.

Figure 7. Temporal variation of q_t vs time at varying dosage and pH 5 for TFC in PE.

Table 3. The kinetic equation used for analysis of kinetic data.

KE	Linear form of the equation	Plots made	Eq. No.	Reference
RFO	$ln(1-U_t) = -k_r$, $U_t = [(C_o-C_t)/(C_t-C_e)]$, $k_r = (K_1 + K_2)$	$ln[1-U_t]$ vs t	3	24, 25
PFO	$log(q_e-q_t) = log\ q_e - (K_s t)/2.303$	$log(q_e - q_t)$ vs t	4	26
PSO	$t/q_t = 1/(k^2 q_e^2) + t/q_e$	t/q_t vs t	5	27
ELV	$q_t = (1/\beta)ln(\alpha\beta) + (1/\beta)lnt$	q_t vs lnt	6	28

Kinetic analysis

Table 3 briefly express the applied kinetic equations and the corresponding plots made. Only pseudo second order plot is shown as Figure 8. The parameters are arrayed in Table 4. Comparison among R^2 shown in Table 4 indicated the following order of variation: pseudo second order > reversible first order > pseudo first order > Elovich. Hence, the pseudo–second order has the best correlation.

Table 4. The kinetic parameters evaluated for TFC in PE at 25 °C and pH 5.

Reversible first order for TFC in PE at 25 °C and pH 5									
Dosage	0.5 g/L	1 g/L	1.5 g/L	2 g/L	2.5 g/L	3 g/L	3.5 g/L	4 g/L	4.5 g/L	5 g/L
K	0.167	0.173	0.181	0.118	0.191	0.193	0.197	0.195	0.196	0.198
R^2	0.9963	0.9979	0.9986	0.9985	0.9991	0.9996	0.9994	0.9997	0.9997	0.9998
Pseudo first order parameters for TFC in PE at 25 °C and pH 5									
Dosage	0.5 g/L	1 g/L	1.5 g/L	2 g/L	2.5 g/L	3 g/L	3.5 g/L	4 g/L	4.5 g/L	5 g/L
K_s (min^{-1})	0.0586	0.0628	0.0676	0.0712	0.0736	0.0754	0.0785	0.0781	0.0791	0.0809
q_e (mg.g^{-1})	572	561.5	544	507	480	489	406	363	325	294
R^2	0.9853	0.9901	0.9923	0.9925	0.9946	0.9963	0.9961	0.9978	0.9983	0.9997
Pseudo second order parameter for TFC in PE at 25 °C and pH 5									
Dosage	0.5 g/L	1 g/L	1.5 g/L	2 g/L	2.5 g/L	3 g/L	3.5 g/L	4 g/L	4.5 g/L	5 g/L
K_2 (g/mg/min)	0.0021	0.002	0.0021	0.0023	0.0025	0.0027	0.0029	0.0033	0.0036	0.0039
q_e (mg/g)	471	467	462	433	395	361	337	304	276	253
h (mg/g/min)	466	437	448	431	389	353	329	304	274	250
R^2	0.9992	0.9995	0.9997	0.9997	0.9998	0.9999	0.9999	0.9999	0.9999	0.9999
Elovich parameters for TFC in PE at 25 °C and pH 5									
Dosage	0.5 g/L	1 g/L	1.5 g/L	2 g/L	2.5 g/L	3 g/L	3.5 g/L	4 g/L	4.5 g/L	5 g/L
B (mg/g.min)	0.296	0.385	0.341	0.441	0.527	0.637	0.768	0.961	1.17	1.47
R^2	0.8660	0.8185	0.8422	0.8047	0.7922	0.7779	0.7657	0.7565	0.7590	0.7289
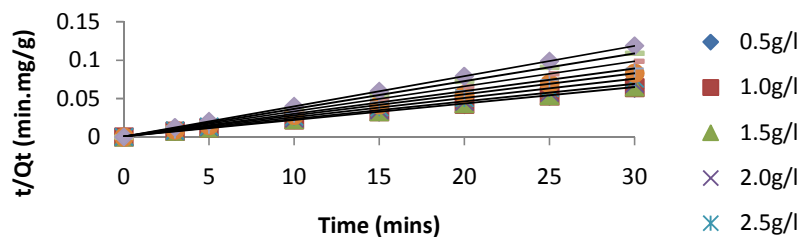
Figure 8. The pseudo-second order kinetic plot for TFC in PE at 25 °C and pH 5.

Intra-particle diffusion kinetics

Weber and Morris model (Eq. 7) investigated intra-particle diffusion resistance on the process [29, 30].

$$q_t = K_{id}\, t^{0.5} \tag{7}$$

where k_{id} (mg.g^{-1}.min$^{-0.5}$) is rate constant, q_t (mg.g^{-1}) is adsorption capacity at time t (min).

The logarithmic form of Eq.7 yields Eq. 8:

$$\mathrm{Log}\, q_t = Log\, K_{id} + 0.5 \mathrm{Log}\,(t) \tag{8}$$

A straight line plot of Eq. 8 with positive intercept is a condition for intra-particle diffusion controlled process. The K_{id} from Figure 9 intercepts are shown in Table 5 for $R^2 > 0.95$, confirming particle diffusion as a rate limiting step.

Model reliability was tested by diffusion coefficient, D_p (Eq. 9) [29, 30]:

$$D_p = (0.03r_o^2)/t_{0.5} \tag{9}$$

where r_0 (4.1425 x 10^{-13} cm) [23] is the average radius of the TFC particles, and $t_{0.5}$ (min) is the half-life of the adsorptive process.

If D_p is in the range 10^{-11} to 10^{-13} cm^2.s^{-1}, then intra-particle diffusion is the rate determining step [30]. Table 5 shows D_p (10^{-16}–10^{-22}cm^2.s^{-1}) that are within 10^{-11} to 10^{-13} cm^2.s^{-1} [30] and $R^2 >$ 0.96, thus confirming intra-particle diffusion as the rate determining step. Similar result has been obtained elsewhere [30].
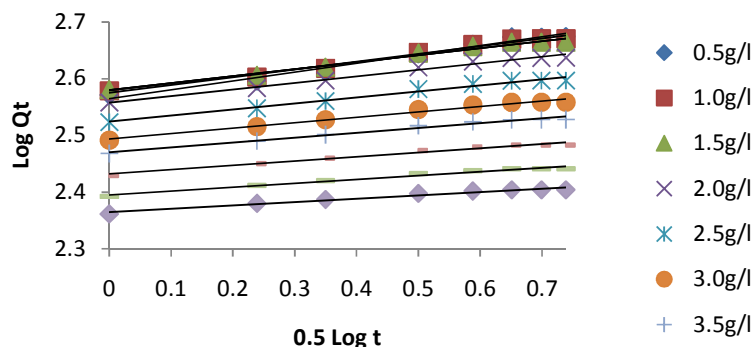

Figure 9. Intra-particle diffusion for TFC in PE at 25°C and pH 5.

Table 5. Intra-particle diffusion parameter for TFC in PE at 25°C and pH 5.

Dosage	0.5 g/L	1 g/L	1.5 g/L	2 g/L	2.5 g/L	3 g/L	3.5 g/L	4 g/L	4.5 g/L	5 g/L
K_{id} (mg/g/min$^{0.5}$)	0.1369	0.1369	0.1235	0.1153	0.1061	0.096	0.0855	0.0757	0.0682	0.0593
Dp (cm^2/s)	1.40 x 10^{-16}	1.80 x 10^{-16}	7.30 x 10^{-17}	3.20 x 10^{-17}	2.80 x 10^{-18}	4.40 x 10^{-19}	2.80 x 10^{-19}	4.50 x 10^{-20}	7.80 x 10^{-21}	4.20 x 10^{-22}
R^2	0.9829	0.9829	0.9843	0.9833	0.9825	0.9812	0.9786	0.9771	0.9756	0.9688

Boyd kinetics

Boyd kinetics equations [30] further confirm the rate-controlling step:

$$F = 1 - \frac{6}{\pi^2}\exp\text{-}\beta t \tag{10}$$
$$F = q_e/q_t$$

$$\beta t = -0.4985 - \ln\left[1 - \left(\frac{q_t}{q_e}\right)\right] \tag{11}$$

where q_t is adsorption capacity at time, t, q_e is adsorption capacity at equilibrium, βt is a mathematical function of $F.q_t$ [30].

Table 6 shows that the R^2 from plot of -βt against time > 0.98. Hence, intra-particle diffusion was the rate determining step. Similar result is reported elsewhere [30].

Table 6. Boyd kinetic parameter for TFC in PE at 25 °C and pH 5.

Dosage	0.5 g/L	1 g/L	1.5 g/L	2 g/L	2.5 g/L	3 g/L	3.5 g/L	4 g/L	4.5 g/L	5 g/L
R^2	0.9853	0.9901	0.9923	0.9925	0.9995	0.9963	0.9961	0.9978	0.9983	0.9983

Isotherm analysis

Table 7 indicates the isotherm models while Figures 10a to c show the equilibrium plots at 25, 35 and 45 °C, respectively. The isotherm data were subjected to linear and non-linear analyses. The parameters are shown in Table 8. The values of R^2, chi-square (χ^2) and sum of square error (SSE) show that the data best fitted with the Langmuir model ($R^2 > 0.99$, $\chi^2 < 1.4$, SSE < 1.6). The data were also fitted to linear models (Figures not shown). Table 9 indicates best fit for the Langmuir ($R^2 > 0.99$, $\chi^2 < 0.6$, SSE < 0.8) and followed by Temkin model. Similar results were obtained in this report where Langmuir isotherm dominated. The Q_{max} increased with increasing temperature. Similar results are obtained for K_F and B.

Table 7. The isotherm model used for the analysis of the equilibrium data.

Model	Non-linear form of the equation	Linear form of the equation	Plots made	Eq. No	Reference
Langmuir	$q_e = (q_m K_a C_e)/(1+K_a C_e)$	$C_e/q_e = 1/(K_a q_m) + C_e/q_m$	$C_e/q_e vs C_e$	12	29-31
Freundlich	$q_e = K_F C_e^{1/n}$	$log q_e = log K_F + (1/n) log C_e$	$log q_e vs log C_e$	13	29-32
Temkin	$q_e = RT/Bt (lnKpCe)$	$qe = (RT/Bt)lnKt + (RT/Bt)lnCe$	$q_e vs lnC_e$	14	21, 25
Frumkin	$q_e = A+Bln(C_e/q_e)$	$q_e vs ln(C_e/q_e)$		15	33
DRK	$q_e = q_s exp(-K_{ad}E^2)$	$lnq_e - lnq_s - K_{ad}E^2$	$lnq_e vs E^2$	16	29, 30

Confirmation of favourability of the adsorptive process

Eq. 17 confirms the favourability of the process for Langmuir [29, 32]:

$$R_L = \frac{1}{(1+KaCo)}$$ (17)

It is: (i) unfavourable when $R_L > 1$, (ii) linear when $R_L = 1$, (iii) favourable when $0 < R_L < 1$, and (iv) irreversible when $R_L = 0$. For Freundlich isotherm, it is favourable if n ranges 1–10. Thus R_L and n values in Tables 8 and 9 indicate favourability.
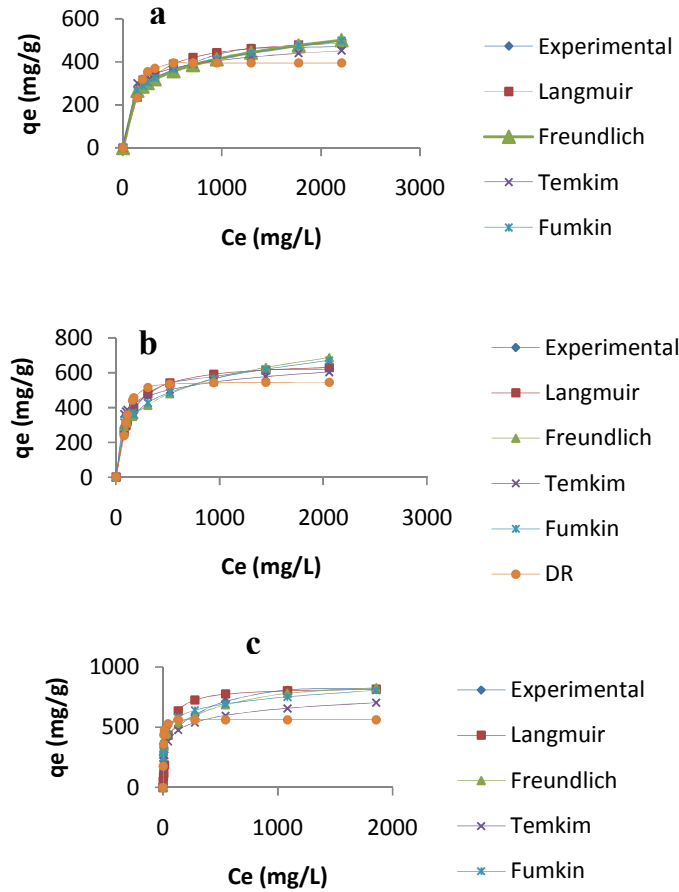
Figure 10. Non-linear isotherm plots of TFC in PE at pH 5 for: (a) 25, (b) 35 and (c) 45 °C.

Adsorption thermodynamics

The (ΔG°), (ΔH°), and (ΔS°), were calculated using Eqs. 18–20, respectively.

$$\Delta G^\circ = -RT \ln K_a \tag{18}$$

$$\Delta H^\circ = R\left[\frac{T_2 T_1}{T_2 - T_1}\right] \ln \frac{K_{a2}}{Ka1} \tag{19}$$

$$\Delta S^\circ = \frac{\left(\Delta H^\circ - \Delta G^\circ\right)}{T} \tag{20}$$

Table 8. The isotherm parameters obtained from non-linear analysis of TFC in PE at pH 5 for Langmuir, Freundlich, Temkin, Frumkin and DRK.

Langmuir	K_a (L/mg)	Q_m (mg/g)	R^2	χ^2	SSE (%)	R_L
25 °C	0.0058	500	0.9975	0.597	1.58	0.06
35 °C	0.0083	667	0.9965	0.625	0.788	0.043
45 °C	0.024	833	0.9959	1.428	0.109	0.015

Freundlich	K_F (L/mg)	N	R^2	χ^2	SSE (%)	
25 °C	82.8	4.27	0.9657	0.152	0.399	
35 °C	92.3	3.81	0.9427	0.272	0.697	
45 °C	226	5.74	0.9850	2.598	6.15	

Temkin	K_T (L/g)	B (kJ/mol)	R^2	χ^2	SSE (%)	
25 °C	1.8	30.0	0.9714	0.0062	0.0855	
35 °C	1.9	24.3	0.9574	0.0151	0.276	
45 °C	2.2	31.5	0.9691	0.2495	1.515	

Frumkin	A	B	R^2	χ^2	SSE	
25 °C	328	109	0.974	8.8195	7.34	
35 °C	492	144	0.901	-28.147	17.7	
45 °C	721	106	0.9634	-42.384	133	

DRK	Q_s (mg/g)	B (mol²/kJ²)	R^2	χ^2	SSE	
25 °C	397	-2.00 x 10⁶	0.522	130429	34474	
35 °C	549	-0.0008	0.868	646	1077	
45 °C	565	-2.00 x 10⁶	0.523	2.00 x 10⁶	2585	

Table 9. The isotherm parameters obtained from linear analysis of TFC in PE at pH 5 for Langmuir, Freundlich, Temkin, Frumkin and DRK.

Langmuir	K_a (L/mg)	Q_m (mg/g)	R^2	χ^2	SSE (%)	R_L
25 °C	0.0056	526	0.9986	0.597	0.757	0.062
35 °C	0.0083	667	0.9997	0.633	0.786	0.043
45 °C	0.024	833	0.9962	0.180	0.146	0.015

Freundlich	K_F (L/mg)	N	R^2	χ^2	SSE (%)	
25 °C	82.0	4.2	0.9668	0.597	0.340	
35 °C	94.4	3.8	0.9518	0.267	0.710	
45 °C	230	5.7	0.9890	2.603	5.17	

Temkin	K_T (L/mg)	B (kJ/mol)	R^2	χ^2	SSE (%)	
25 °C	1.6	29.0	0.9812	0.334	3.69	
35 °C	1.7	22.5	0.9579	0.849	7.64	
45 °C	1.9	30.4	0.9701	1.559	9.79	

Frumkin	A	B	R^2	χ^2	SSE	
25 °C	327	111	0.9644	8.60	7.14	
35 °C	492	149	0.9040	-28.7	16.8	
45 °C	720	105	0.9654	-41.0	135	

DRK	Q_s (mg/g)	B (mol²/kJ²)	R^2	χ^2	SSE	
25 °C	394	-0.000002	0.5256	133143	3439	
35 °C	545	-0.0008	0.8782	660	1078	
45 °C	562	-0.00001	0.5313	168687	2587	

Parameters values are presented in Table 10. Positive $\Delta H^{°}$ indicated endothermicity, while positive $\Delta S^{°}$ pointed to increased randomness [26, 29]. $\Delta G^{°}$ values were increasingly negative, indicating increasing feasibility and spontaneity. The process was physiosorption since $\Delta H^{°}$ (47.3 kJ/mol) is below the threshold of 40 kJ/mol. Thus, van der Waals attraction prevailed. A similar result has been reported elsewhere [21].

Table 10. Thermodynamics parameters of TFC in PE.

T (K)	$\Delta G^{°}$ (kJ/mol)	$\Delta H^{°}$ (kJ/mol)	$\Delta S^{°}$ (kJ/mol)	E_a (J/mol)
298	-28.8			
308	-30.8	47.3	0.256	30.0
318	-34.6			

CONCLUSION

Particle removal was a function of dosage, pH and settling time. Optimum efficiency of 97% was obtained at pH 5 and 2 g/L. Kinetic data best correlated with the pseudo-second order equation, q_t increased with increasing temperature. Equilibrium data fitted the Langmuir model best. Thermodynamics showed endothermic and spontaneous process. The adsorptive process was a significant component in the coagulation process. This was shown by significant fitting of coagulation data to adsorption model equations, coupled with high performance of TFC at the experimental conditions.

ACKNOWLEDGEMENTS

REFERENCES

1. Akyol, A. *Desalination* **2012**, 285, 91.
2. Aydin, S.; Yasin, O.B. *Desalin. Water Treat*. **2016**, 57, 12692.
3. Menkiti, M.C.; Ndaji, C.R.; Ezemagu, I.G.; Oyoh, K. B.; Menkiti, N.U. *J. Environ. Chem. Eng*. **2015**, 3, 1802.
4. Swati, M.; Govindan. V.S. *J. Indian Water Works Assoc*. **2005**, 37, 145.
5. Menkiti, M.C.; Ezemagu, I.G.; Nwonye, C.I.; Ejimofor, M.I. *Int. J. Energy Environ. Eng*. **2015**, Doi 10.1007/S40095-015-0192-Y.
6. Menkiti, M.C.; Nnaji, P.C.; Onukwuli, O.D. *Nat. Sci*. **2009**, 7, 1.
7. Simate, G.S.; Iyuke, S.E.; Ndlovu, S.; Heydenrychb, M. *Wat. Res*. **2012**, 46, 1185.
8. Menkiti, M.C. *Studies on the Rapid Coagulation and Flocculation of Coal Washery Effluent: A Turbidimetric Approach*, M.Sc Thesis, Nnamdi Azikiwe University, Awka, Nigeria, **2007**.
9. Verma S.; Prasad, B.; Mishra, I.M. *J. Hazard. Mater*. **2010**, 178, 1055.
10. Menkiti, M.C.; Nwonye, C.I.; Onyechi, C.A.; Onukwuli, O.D. *Adv. Chem. Eng. Sci*. **2011**, 1, 125.
11. Renault, F.; Sancey, B.; Badot, P.M.; Crini, G. *Eur. Polym. J*. **2009**, 45, 1337.
12. Verma, A.K. Das, R.R.; Bhunia, P. *J. Environ. Manage*. **2012**, 93, 154.
13. Menkiti, M.C.; Onukwuli, O.D. *AICHE Journal*, **2012**, 56, 1303.

14. Miller, S.M.; Fugate, E.J.; Craver, V.O.; Smith, J.A.; Zimmerman, J.B. *Environ. Sci. Technol.* **2008**, 42, 4274.

15. Clesceri, L.S.; Greenberg, A.E.; Eaton, A.D. *Standard Methods for the Examination of Water and Wastewater*, 20th Edition, American Public Health Association (APHA): USA; **1999**.

16. Feng, Y.; Gong, J.; Zeng, G.; Niu, Q.; Zhang, H.; Niu, C.; Deng, J.; Yan, M. *J. Chem. Eng.* **2010**, 162, 487.

17. Menkiti, M.C.; Ndaji, C.R.; Ezemagu, I.G.; Udammeri, V. *J. Disper. Sci. Technol.* **2015**, 37, 760.

18. Stuart, B.H. *Infrared Spectroscopy: Fundamentals and Applications*, John Wiley and Sons: New York; **2004**.

19. Menkiti, M.C.; Ezemagu, I.G.; Okolo, B.I. *Pet. Sci.* **2016**, 13, 328.

20. Gill, P.; Moghadam, T.; Ranjbar, B. *J. Biomol. Tech.* **2010**, 21, 167.

21. Menkiti, M.C.; Aneke, M.C.; Ejikeme, P.M.; Onukwuli, O.D.; Menkiti, N.U. *Springerplus* **2014**, 3:213.

22. Ramani, K.; Jain, S.C.; Mandal, A.B.; Sekaran, G. *Colloids Surf. B: Biointerfaces* **2012** 97, 254.

23. Ezemagu, I.G. *Nephlometric Study of Adsorptive and Non-Adsorptive Components of Coagulation of Produced Water and Paint Effluent Using Bioextracts*, M.Sc Dissertation, Nnamdi Azikiwe University, Awka, Anambra State, Nigeria, **2015**.

24. Deng, S.; Bai, R. *Water SA* **2005**, 31, 597.

25. Kannan, A.; Thambidurai, S. *Bull. Chem. Soc. Ethiop.* **2008**, 22, 183.

26. Mohan, D.; Singh, K.P.; Singh, V.K. *J. Hazard. Mater.* B 2006, 135, 280.

27. Wong, Y.C.; Szeto, Y.S.; Cheung, W.H.; Mckay, G. *J. Appl. Polym. Sci.* **2004**, 92, 2054.

28. Khan, M.I.; Khan, M.A.; Zafar, S.; Hussain, S.A. *Sch. J. Eng. Tech.* **2015**, 3, 741.

29. Adeno, F.; Mulugeta, E.; Zewge, F.; Chebude, Y. *Bull. Chem. Soc. Ethiop.* **2014**, 28, 215.

30. Debnath, S.; Ghosh, U.C. *J. Chem. Thermodyn.* **2008**, 40, 67.

31. Ahmet, S.; Ömer, I. *Bull. Chem. Soc. Ethiop.* **2006**, 20, 259.

32. Qin, L.; Jianping, Z.; Wenyi, Z.; Mingmei, W.; Jun Z. *Bull. Chem. Soc. Ethiop.* **2008**, 22, 19.

33. Volkova-Gugeshashvili, M.I.; Volkov, A.G.; Markin V.S.R. *J. Electrochem.* **2006**, 42, 1073.